

# Nanostructured Pd Hydride Microelectrodes: In Situ Monitoring of pH Variations in a Porous Medium

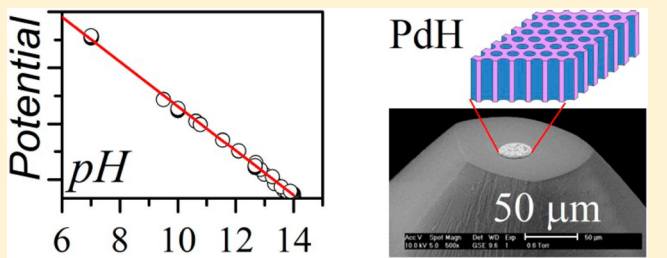
Mara Serrapede,<sup>†</sup> Giovanni Luca Pesce,<sup>‡</sup> Richard J. Ball,<sup>‡</sup> and Guy Denuault\*,<sup>†</sup>

<sup>†</sup>School of Chemistry, University of Southampton, SO17 1BJ Southampton, U.K.

<sup>‡</sup>Department of Architecture & Civil Engineering, University of Bath, BA2 7AY Bath, U.K.

## Supporting Information

**ABSTRACT:** In this study we report the exceptional potentiometric properties of pH microprobes made with nanostructured palladium hydride microelectrodes and demonstrate their application by monitoring pH variations resulting from a reaction confined in a porous medium. Their potentiometric response was found to be reproducible and stable over several hours but primarily Nernstian over a remarkably wide pH range, including alkaline conditions up to pH 14. Continuous operation was demonstrated by reloading hydrogen at regular intervals to maintain the correct hydride composition thereby alleviating the need for calibration. These properties were validated by detecting pH transients during the carbonation of  $\text{Ca}(\text{OH})_2$  within a fibrous mesh. Experimental pHs recorded *in situ* were in excellent agreement with theoretical calculations for the  $\text{CO}_2$  partial pressures considered. Results also showed that the electrodes were sufficiently sensitive to differentiate between the formation of vaterite and calcite, two polymorphs of  $\text{CaCO}_3$ . These nanostructured microelectrodes are uniquely suited to the determination of pH in highly alkaline solutions, particularly those arising from interfacial reactions at solid and porous surfaces and are thus highly appropriate as pH sensing tips in scanning electrochemical microscopy.



Numerous chemical reactions involve pH changes but despite its importance pH still remains a difficult parameter to determine in many cases. On the one hand, extreme pHs cannot be measured reliably with most pH sensitive devices, including the conventional glass electrode. On the other hand, pH is hard to measure in confined places with interfacial processes typically found in geochemistry, electrochemistry, or biochemistry proving to be particularly challenging. Of all the pH sensors currently available, the glass electrode is by far the most convenient for measurements in bulk solutions but it is unsuited for operations in localized environments. It is also unsuited to very basic media, as the alkaline error (a phenomenon also known to worsen with temperature<sup>1</sup>) affects the response for  $\text{pH} > 9$ ; even with alkaline glass membranes,<sup>2</sup> its response becomes unreliable above pH 12. While strong alkaline conditions are common in industrial processes (e.g., in the treatment of cellulose for the production of pulp or of nuclear waste to precipitate oxides),<sup>3</sup> many interfacial processes also produce high pHs (e.g., electrochemical reductions often involve the consumption of protons and locally generate alkaline conditions).<sup>4–6</sup> High pHs are also common in geochemistry (e.g., in geopolymers<sup>7</sup> but also in many cementitious materials where pore waters have pHs over 13).<sup>8,9</sup>

The requirement for highly localized pH measurements in biological research and the need to overcome difficulties in fabricating miniaturized glass pH electrodes led to the construction of pH microsensors based on metal–metal oxide

equilibria. Antimony<sup>10</sup> and tungsten<sup>11</sup> are often exploited because of their relatively low melting point, ease of use, and the availability of high-purity substrates, but they can only operate between pH 2 and pH 12.<sup>12–16</sup> Many pH electrodes are based on an electrodeposited iridium oxide film<sup>17</sup> covered with Nafion<sup>18</sup> to decrease the interference from anionic redox species, but their operational range is limited to pH 2–11.<sup>19,20</sup> Several pH sensitive electrodes are based on titanium compounds. The TiN electrode shows two different, nearly Nernstian, slopes at pH 2–12 and 11–14.<sup>21</sup> The  $\text{IrO}_x\text{-TiO}_2$  electrode shows a Nernstian response between pH 1 and pH 13.<sup>22</sup> The ruthenium dioxide electrode shows a linear response from pH 2 to pH 12.<sup>23</sup> A pH electrode consisting of a  $\text{PbO}_2$  paraffin matrix deposited on graphite has been proposed by Lima et al. for pH 1.2 to pH 7.5.<sup>24</sup> A sensitive pH electrode based on solid state  $\text{PbO}_2$  film electrodeposited on a carbon ceramic electrode was reported by Razmi et al.<sup>25</sup> to have a near Nernstian slope between pH 1.5 and pH 12.5. A silica sol–gel derived zeolite-graphite composite pH electrode with zeolite as proton receptor<sup>26</sup> showed a Nernstian response from pH 1 to pH 12. Measurements between pH 8 and pH 13 were reported with a hydroxide-selective electrode made of 10%  $\text{Cu}_2\text{S}$  and 90% of  $\text{Ag}_2\text{Se}$ .<sup>27</sup> Proton-specific ion selective electrodes (ISE) have also been produced with liquid ion-exchange resins doped

Received: January 23, 2014

Accepted: May 12, 2014

Published: May 12, 2014

with a proton specific ionophore (see reviews by Buhlman et al).<sup>28,29</sup> Oesch et al.<sup>30</sup> proposed 11 neutral hydrogen ionophores to produce ion-selective electrodes for distinct pH ranges. The range depends on the  $pK_a$  of the ionophore incorporated in the membrane; most membranes operate from mildly acidic to mildly alkaline pH and extremes are once again hard to measure. Membranes made with derivatives of propyl red cover the pH range 1–10, while those made with tridodecylamine cover the range 4–12.<sup>29</sup> Optical pH sensors are increasingly exploited, but their operational range is typically limited to pHs between 5 and 9 with commercially available dyes; sensing from pH 2 to 12 is possible with dyes possessing two  $pK_a$  values or when combining dyes with different  $pK_a$ 's.<sup>31</sup> Finally solid Pd electrodes have been used to monitor pH potentiometrically.<sup>2</sup> For this, the Pd must be loaded with hydrogen to a H to Pd ratio corresponding to the  $\beta$  to  $\alpha$  phase transition of the Pd hydride (PdH).<sup>32</sup> Under these conditions, the PdH electrode takes a potential linearly related to pH. Being solid and fabricated without glass, PdH electrodes have been used to monitor pH in the presence of strong fluoride concentrations<sup>33–35</sup> and at elevated temperatures and pressures.<sup>36</sup>

Among all these approaches, the palladium hydride electrode stands out as the only one capable of producing a single Nernstian response over the whole pH range.<sup>37</sup> It can be turned into a microdisk electrode to perform localized measurements, but its potentiometric response is not stable with time as the hydrogen diffuses in to the bulk of the Pd wire. To circumvent this problem, Imokawa et al.<sup>38</sup> electrodeposited thin nanostructured Pd films onto Pt microdisks and showed that, once loaded with H, the PdH film exhibited a single Nernstian response from pH 2 to 12. They also showed that the electrodes were robust, accurate, and able to deliver highly reproducible results thanks to their huge electroactive area. The latter, typically a few hundred times larger than the geometric area of the underlying Pt disk, allows the electrodes to be miniaturized to micrometer dimensions without compromising the stability of the potentiometric response. Imokawa et al. also reported that the lifetime of the nanostructured PdH microdisks was seriously shortened by the presence of dissolved oxygen. Recently, we have shown that the presence of oxygen also affects the potentiometric response where, instead of delivering a potential proportional to pH, the electrodes produce a mixed potential related to pH and to the flux of oxygen toward the electrode as it reduces on the nanostructured Pd film.<sup>39</sup> In short, the greater the flux of oxygen toward the electrode, the shorter the lifetime of the sensor and the more its potential is offset from the Nernstian response expected in absence of oxygen. Both of these effects were found to be pronounced with micrometer size electrodes (large rates of steady-state mass transport) but negligible with large electrodes (low rates of mass transfer).

In this study, we describe how nanostructured Pd hydride microelectrodes were successfully exploited to monitor pH variations from a reaction confined in a porous substrate with solutions ranging from very alkaline to mildly acidic. Through calibrations, we first demonstrate that the Nernstian potentiometric pH characteristic of the microelectrodes extends to strong alkaline conditions. We then describe how the electrodes were successfully employed to record pH transients during the carbonation of lime within a humid fibrous mesh. Having performed the experiments with different partial pressures of CO<sub>2</sub> to control the carbonation, we validate the experimental

results with theoretical calculations from PHREEQC,<sup>40</sup> with SEM observations and with XRD analysis of the CaCO<sub>3</sub> particles deposited on the mesh fibers. The carbonation of lime was chosen not only to illustrate the application of the microelectrodes for in situ measurements but also because its acid–base equilibria made it possible to compare experimental results with theoretical calculations. With this example we also intended to demonstrate that these electrodes could be exploited to record interfacial pH near solid or porous electrodes and thus be easily turned into pH sensing tips for scanning electrochemical microscopy.

## ■ EXPERIMENTAL SECTION

The pH microelectrodes were fabricated and characterized as reported previously.<sup>38,41</sup> Briefly, nanostructured palladium films were electrodeposited under potentiostatic control at 0.1 V vs SMSE, on Pt microdisks from a plating mixture consisting of (NH<sub>4</sub>)<sub>2</sub>PdCl<sub>4</sub> 12 wt % (Alfa Aesar, premion-99.998%), C<sub>16</sub>EO<sub>8</sub> 48 wt % (octaethylene glycol monohexadecyl ether, Fluka), heptane 2 wt % (Lancaster, 99%) and water 40 wt % (18 MΩ cm, PurIte, Burkert). These conditions were chosen to use the hexagonal phase of C<sub>16</sub>EO<sub>8</sub>, a nonionic surfactant known to form liquid crystal phases,<sup>42</sup> as a molecular template to direct the deposition of the Pd and produce the desired nanostructure. To guarantee the presence of the hexagonal phase of the surfactant, the plating mixture was annealed at 40 °C for 30 min, manually stirred, and placed in an ice bath for 30 min. This process was repeated before allowing the mixture to cool to room temperature. Electrodeposition was carried out at room temperature with small volumes from the stock mixture. The latter was kept for up to 3 weeks with the annealing–cooling process undertaken before each use. Where required, the hexagonal phase of the surfactant template was confirmed by polarization microscopy as reported previously.<sup>41</sup> The films were deposited on Pt microdisks with diameters ranging from 25 to 250 μm with a charge  $Q_{dep} = 4 \text{ C cm}^{-2}$ , such that the film thickness was typically 1 to 2 μm. Pt was chosen as a substrate to prevent the loss of hydrogen by diffusion from the hydride into the substrate. The electrodes were then soaked in water for at least 24 h to remove the surfactant, and the Pd films were activated by cyclic voltammetry in sulfuric acid until stable voltammograms characteristic of Pd<sup>41</sup> were obtained. The Pd films were then galvanostatically loaded with hydrogen (−80 nA for the 25 μm diameter disks up to −60 μA for the 250 μm diameter disks) to a H/Pd ratio ca. 0.6 corresponding to the beginning of the  $\beta$  PdH phase. In practice, loading was stopped when the potential dropped below the plateau for the  $\alpha$  to  $\beta$  phase transition. Hydrogen loading was generally performed in the solution of interest at regular intervals or whenever H needed replenishing. Sensitivity to pH was obtained by recording the electrode potential, while the PdH was in its  $\beta$  to  $\alpha$  transition; under these conditions, the phase rule dictates that the hydride behaves as a hydrogen electrode with a Nernstian dependence of potential on pH.<sup>2</sup> The microelectrodes were used as pH sensors by recording their open circuit potential ( $OCP_{\beta \rightarrow \alpha}$ ) until the natural discharge of hydrogen had taken the hydride into its  $\alpha$  phase. The electrodes have two characteristic times  $t_1$  and  $t_2$  such that for  $t < t_1$  the hydride is in the  $\beta$  phase; for  $t_1 < t < t_2$  the  $\beta$  and  $\alpha$  phases are both present in the hydride, and for  $t > t_2$  the hydride is in its  $\alpha$  phase (see Figure SI-1 of the Supporting Information for a typical chronopotentiogram). The electrodes can only be used as pH sensors between  $t_1$  and  $t_2$ , and from

now on,  $t_2 - t_1$  will be called the lifetime of the pH sensor. The electrode potential was measured against a homemade saturated mercury sulfate electrode (SMSE). To minimize electrical noise, all experiments were performed in a grounded Faraday cage. Under these conditions,  $OCP_{\beta \rightarrow \alpha}$  is very stable, typically fluctuating  $\pm 1.5$  mV, and its value can be linearly related to the pH. The electrochemical experiments were performed with a PGSTAT101 operated with Nova 1.9, both from Eco Chemie. Calibration curves were obtained by recording the electrode potential in different solutions prepared with buffers or via neutralization of a strong base. The buffers were made with  $H_3PO_4$  (Fischer Scientific, 86%),  $NaH_2PO_4 \cdot 2H_2O$  (Fisher Scientific, 99.2%),  $Na_2HPO_4 \cdot 12H_2O$  (BDH, Analar),  $Na_2SO_4$  (Merck, 99.99%), NaOH (Fisher Scientific, 97%), and  $H_2SO_4$  (Fisher Scientific, 95%), according to the recipes of Beynon and Easterby for thermodynamically correct buffers.<sup>43</sup> The acid components were  $H_3PO_4$  for  $1.15 \leq pH \leq 3.15$ ,  $NaH_2PO_4 \cdot 2H_2O$  for  $6.2 \leq pH \leq 8.2$ , and  $Na_2HPO_4 \cdot 12H_2O$  for  $11.5 \leq pH \leq 13.5$ . In all cases, the base component was NaOH and  $Na_2SO_4$  was added to fix the ionic strength to 200 mM. The pH was then finely tuned to the desired level with small aliquots of 0.1 M NaOH. As the buffers were prepared at room temperature but used at 25 °C, the pH of each buffer was rerecorded in a water-jacketed cell at  $25 \pm 0.5$  °C with a pH meter (HI111 and HI2213, both from Hanna Instruments) and a glass electrode pH probe (HI1131B, pH 0 to 13 and HI1043B, pH 0 to 14, both from Hanna Instruments). The pH meters were regularly calibrated at 25 °C with standard buffers (HI7010, pH =  $10.01 \pm 0.01$ ; HI7007, pH =  $7.01 \pm 0.01$ ; and HI7004, pH =  $4.01 \pm 0.01$ , all from Hanna Instruments). Above pH 12, the calibration solutions were prepared by neutralizing 1 M NaOH and 1 M NaOH + 50 mM  $Na_3PO_4 \cdot 12H_2O$  (Sigma-Aldrich, 99.0%) solutions with 5, 1, and 0.1 M solutions of  $H_2SO_4$  and calculating the pH theoretically. NaOH (1 M) was used for pH 14. For each calibration solution, the potential of the nanostructured microdisk was recorded at 25 °C in the bulk and after purging with Ar (Pureshield, BOC) for 10 min.

Experiments to investigate the carbonation of lime were carried out with saturated solutions of  $Ca(OH)_2$  (produced by decomposition of pure  $CaCO_3$ , Sigma-Aldrich  $\geq 99.0\%$ , subsequently hydrated in deaerated water) absorbed in small strips (3 mm wide  $\times$  1 cm long) of cotton linter (a cellulose lens cleaning paper, Whatman) inside a homemade poly(methyl methacrylate) (PMMA) cell (Figure 1) under thermostatic conditions (23 °C) and with different Ar/CO<sub>2</sub> gas mixtures. The cotton mesh was used for three reasons: to trap a thin film of solution and thus simulate carbonation in the confinement of a porous medium, to provide an ionic path between the electrodes, and to capture the solid phases formed during the carbonation for subsequent analysis. The reference electrode was clamped outside the cell and connected to the solution via a salt bridge (Agar saturated with  $K_2SO_4$ , Difco) attached to the body of the microelectrode and terminated by a capillary tip flushed with that of the microelectrode. This configuration was implemented to guarantee a constant distance between the pH sensing tip and the reference electrode and thus avoid Ohmic distortion while galvanostatically loading the microelectrodes with hydrogen. The cell contained up to 3 mL of solution and had a removable lid (inset in Figure 1) designed to clamp the counter electrode at the bottom of the cell and prevent any movement during the tests. The two long side walls of the cell were made from glued

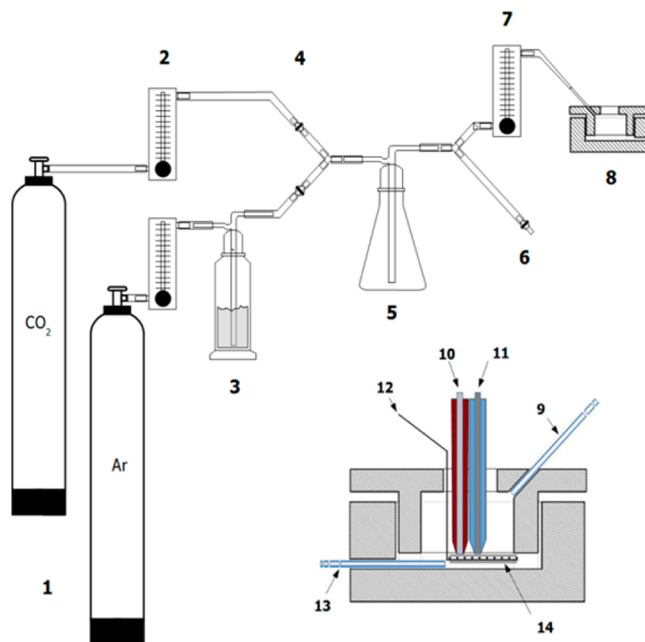


**Figure 1.** Schematic of the experimental assembly. (1) gas cylinders, (2) gas flow meters, (3) humidifier, (4) valves, (5) mixing chamber, (6) exhaust line and valve, (7) flow meter and regulator, (8) cell detailed in the inset below, (9) gas mixture injector, (10) reference electrode salt bridge, (11) pH sensing electrode, (12) counter electrode, (13) capillary to remove the solution, and (14) cellulose mesh.

microscope slides to facilitate inspection of the mesh and electrodes positions. The pH sensing electrode and attached salt bridge were introduced into the cell after closure of the lid, through a circular opening in the lid. At the bottom of the cell, a plastic capillary was connected to a syringe to allow the removal of the solution. Gas mixtures were introduced into the cell via a glass pipet inserted through a second hole in the lid. The gas mixtures, oxygen free Ar and CO<sub>2</sub> (Pureshield from BOC), were streamed into the cell through a thermostated humidifier (pure water) to ensure the mesh never dried out. Specific  $p_{CO_2}$  were obtained by adjusting the valves and flow meters detailed in Figure 1. Each cylinder was connected to a flow meter that allowed a specific flow for each gas and, consequently, a specific volume or partial pressure. The gas blend was homogenized in a mixing chamber and the stream was split between an exhaust line and a feed line regulated by a flow meter set at  $0.25 \text{ L min}^{-1}$ . The exhaust valve was adjusted to avoid gas overpressure within the system. A typical experiment was conducted as follows: (1) the mesh was wrapped around the counter electrode. (2) The electrodes were positioned in the cell and clamped with the lid. (3) A stream of wet Ar was passed into the cell. (4) The cell was filled with approximately 3 mL of saturated  $Ca(OH)_2$  solution using a syringe fitted with a disposable filter (0.1  $\mu\text{m}$  Puradisc 25 TF from Whatman) to avoid introducing solid phases. (5) Cyclic voltammograms were recorded to establish the cleanliness of the Pd nanostructure. (6) A chronopotentiogram was recorded while loading the palladium film galvanostatically with hydrogen to a H/Pd ratio ca. 0.6 corresponding to the beginning of the  $\beta$  phase of the hydride. (7) The microelectrode was set to open circuit, and its potential was recorded to measure the pH in the bulk of the solution. (8) While continuously recording its potential, the microelectrode was moved downward until its tip

touched the cellulose mesh. (9) After checking for signal stability, the solution was removed from the cell using the syringe and capillary at the bottom of the cell, thereby leaving some solution absorbed in the cellulose mesh. (10) The baseline pH for the thin film of solution was recorded. (11) The gas mixture was modified to allow a chosen partial pressure of humid CO<sub>2</sub> in the cell. (12) The electrode potential was recorded continuously while carbonation occurred until a stable plateau was reached. The solid phases precipitated within the mesh samples were subsequently observed with a field emission scanning electron microscope (model FESEM6301F from JEOL) and analyzed with an X-ray diffractometer (Rigaku Smartlab with a 9 kW source and Cu k-alpha X-rays).

## THEORETICAL CALCULATIONS

Obtained from the microelectrode potentials during the carbonation of lime, pHs were compared with theoretical values calculated with PHREEQC v. 3.0, a computer program which simulates chemical equilibria, reactions, and transport processes in aqueous media using thermodynamic tables and interactions between liquid, solid, and gas phases.<sup>40</sup> The software is used to model geochemical processes typically found in hydrology and environmental pollution and to predict phase transformation, as in the recent study of the evolution of the phase and morphology of calcium carbonate precipitated by carbonation of hydrated lime.<sup>44</sup> Simulations followed previously reported PHREEQC protocols<sup>45</sup> with an initial condition consisting of one solution in equilibrium with two phases. A solution consisting of 1 kg of pure water (set by default to pH = 7 and pe = 4, i.e., to a redox potential of 0.237 V vs SHE) was used as the solvent with additions of calcium to simulate the saturated lime. pH was set as an adjustable parameter to achieve charge balance, and calculations were carried out for three temperatures: 20, 23, and 25 °C. The equilibrium phases were gaseous CO<sub>2</sub> and one of the solid polymorphs of calcium carbonate. Following the instructions provided with the software, the log of p<sub>CO<sub>2</sub></sub> (in bar) was set to simulate carbonation under different atmospheres. The number of moles of carbon dioxide was set to 1000 to model the equilibrium with an infinite reservoir of CO<sub>2(g)</sub>. Solid phases considered (monohydrocalcite, vaterite, aragonite, or calcite) were modeled using a saturation index of 0 and an infinite number of moles (although similar results were obtained without considering the number of moles of solid phase introduced). Simulations were performed with the thermodynamic data from the Lawrence Livermore National Laboratory database (the LLNL database built in PHREEQC) of Berkeley, which was modified by adding data for vaterite taken from the SIT database (also built in PHREEQC) developed for the French National Radioactive Waste Management Agency. The PHREEQC input files are shown in Supporting Information.

## RESULTS AND DISCUSSION

**Analytical Characteristics.** Figure 2 shows a typical calibration curve recorded with a 25 μm diameter pH probe. The open circuit potential for the β→α transition of the hydride, OCP<sub>β→α</sub>, is found to be linearly related to the pH of the solution over the pH range considered, and the slope of the linear fit, 58.7 ± 0.5 mV pH<sup>-1</sup>, is in excellent agreement with that recorded by Imokawa et al.<sup>38</sup> Figure 2 clearly shows that the Nernstian response of the nanostructured PdH microelectrodes extends to very alkaline conditions and that the

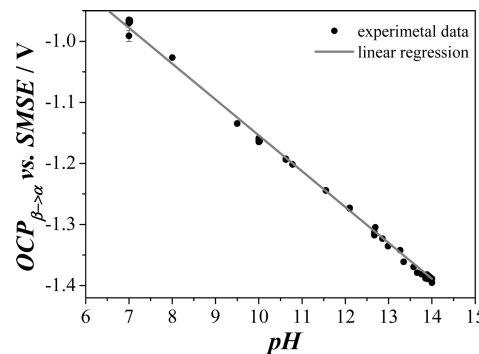


**Figure 2.** Potential-pH calibration for a 25 μm diameter nanostructured PdH-pH probe. Each potential is the average of at least three recordings. Each pH was prepared with different buffers or through partial neutralization of NaOH, as described in Experimental Section.

reproducibility is not affected by high pHs (error bars are comparable to or smaller than the size of the symbols on the curve). We are not aware of previously reported reliable pH measurements with electrodes to such high pH (Imokawa et al.<sup>38</sup> had reported their results up to pH 12). The fact that these data were recorded with micrometer size electrodes indicates how much the potentiometric properties of the Pd film are improved by the nanostructure. Interestingly, the probes produced a stable response over at least 2 h of continuous monitoring (after that hydrogen needed to be reloaded to the beginning of the β phase) and could be used for 14 consecutive days before renewing the nanostructure. The quality of the nanostructure was monitored regularly by voltammetry in sulfuric acid, and in general, the nanostructure was renewed after 60 reloading events. Between experiments, the nanostructured Pd microdisks were kept immersed in pure water. Stored in this way, the nanostructured Pd electrodes could be preserved for several months. Although not systematically investigated, their shelf life is remarkable as some microelectrodes older than one year still worked as pH sensors as soon as they were reloaded with H to the correct hydride composition. The nanostructure was reported to be unaffected by the hydrogen insertion/extraction process,<sup>41</sup> despite a ca. 10% expansion of the Pd lattice during the α to β transition.<sup>46</sup> Similarly, the nanostructure was not affected by aggressive solutions (e.g., 1 M H<sub>2</sub>SO<sub>4</sub> or NaOH), but frequent voltammetric cycling of the electrodes between the foot of hydrogen evolution and the foot of oxygen evolution was avoided as the repeated formation and reduction of Pd oxide gradually destroys the nanostructure.<sup>41</sup> The response time of the electrodes was not investigated, but previous experiments with the substrate generation-tip collection mode of the scanning electrochemical microscope showed that the response time of the nanostructured PdH electrodes to a change in pH was better than 0.6 s.<sup>47</sup>

**Theoretical Calculations for the Neutralization of Saturated Ca(OH)<sub>2</sub> Solutions.** In accordance with PHREEQC calculations (Table 1), the initial pH of saturated Ca(OH)<sub>2</sub> solutions at 20, 23, and 25 °C is 12.56, 12.45, and 12.37, respectively. After carbonation, the final pH varies from a minimum of 6.08 for a solution in equilibrium with calcite at 25 °C and p<sub>CO<sub>2</sub></sub> = 0.75 atm to a maximum of 7.21 for a solution in equilibrium with monohydrocalcite at 23 °C and p<sub>CO<sub>2</sub></sub> = 0.038 atm. At 23 °C, the final pH of the solution in equilibrium with calcite varies from 6.08 to 6.92, depending on p<sub>CO<sub>2</sub></sub>. Simulations

**Table 1.** Theoretical pH Values Calculated with PHREEQC v. 3.0 for the Carbonation of Saturated  $\text{Ca}(\text{OH})_2$  solutions under Different Temperatures,  $\text{CO}_2$  Partial Pressures, And Resulting Solid Phases

$p_{\text{CO}_2}$ (atm)	final pH at 20 °C (initial pH = 12.56)			
	monohydrocalcite	vaterite	aragonite	calcite
0.750	6.389	6.317	6.139	6.087
0.167	6.805	6.734	6.559	6.508
0.039	7.215	7.154	6.972	6.921
final pH at 23 °C (initial pH = 12.45)				
$p_{\text{CO}_2}$ (atm)	monohydrocalcite	vaterite	aragonite	calcite
0.750	6.338	6.310	6.135	6.083
0.167	6.805	6.728	6.555	6.504
0.039	7.214	7.139	6.968	6.917
final pH at 25 °C (initial pH = 12.37)				
$p_{\text{CO}_2}$ (atm)	monohydrocalcite	vaterite	aragonite	calcite
0.750	6.388	6.306	6.132	6.080
0.167	6.805	6.724	6.553	6.501
0.039	7.214	7.135	6.966	6.915

show that the pH is more acidic in the presence of calcite compared to other solid phases and that it takes more neutral values with the less stable phases (respectively, aragonite, vaterite, and monohydrocalcite). Aragonite produces pH values similar to those obtained with calcite, while monohydrocalcite produces pH values closer to those obtained with vaterite. The simulations show that between 20 and 25 °C, temperature has little effect on the final pH of the solutions. The smallest difference was found between the pH of two solutions at 20 and 25 °C containing monohydrocalcite (0.001 pH), while the largest difference was found between the solutions containing vaterite (0.011 pH).

**In situ Monitoring of Lime Carbonation within a Porous Substrate.** To demonstrate the ability of the nanostructured microelectrodes to monitor pH in confined spaces, we followed the pH during the carbonation of a saturated  $\text{Ca}(\text{OH})_2$  solution trapped in the pores of a cellulose mesh, as described in Experimental Section. The microelectrode was initially located in the bulk of the Ar purged saturated  $\text{Ca}(\text{OH})_2$  solution. Figure 3 shows a potential transient recorded from the formation of the  $\beta$  phase of the Pd hydride (i.e., just after the nanostructured Pd electrode was loaded with hydrogen), until the carbonation inside the mesh was complete. The first 30 min of the chronopotentiogram show a rise in potential that reflects the loss of hydrogen from the  $\beta$  phase of the hydride. The plateau appears when the  $\alpha$  phase begins to nucleate and lasts while the two phases coexist; under this condition, the phase rule states that the electrode potential is independent of the Pd hydride composition and solely determined by the pH. At point A shown in the inset, ca. 45 min from the beginning of the experiment, the microelectrode was moved downward until it touched the mesh; this did not affect the potentiometric response. At point B (ca. 47 min), the solution was removed from the cell using the syringe; this had no effect on the microelectrode potential and clearly indicates that the microelectrode was able to monitor the pH of the saturated  $\text{Ca}(\text{OH})_2$  solution trapped within the mesh. At that stage, the solution was still saturated with Ar and its pH was therefore defined by the lime saturation. In accordance with the calibration curve shown in Figure 2, the pH at point B is 12.45 ( $\text{OCP}_{\beta \rightarrow \alpha} = -1.295 \text{ V}$ ). This value is quite different

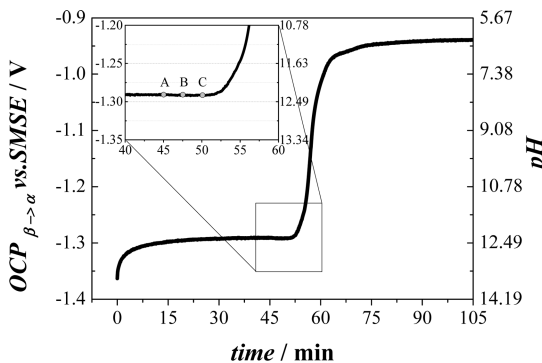
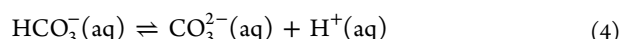
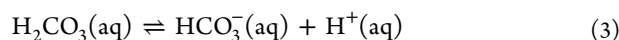


**Figure 3.** Potential transient recorded with a 250  $\mu\text{m}$  diameter nanostructured PdH disk during the carbonation of a saturated  $\text{Ca}(\text{OH})_2$  solution trapped inside a cellulose mesh. The pH axis was calculated from the open circuit potential axis on the left and the calibration curve shown in Figure 2. The inset shows the same data with A, B, and C, respectively, indicating when the working electrode touched the surface of the porous medium, the removal of the solution, and the insertion of the  $\text{CO}_2$  in the gas stream.

from the pH 12.7 measured with the glass electrode of a conventional pH meter (Lutron Soil pH Meter PH-220S with combination glass electrode PE-06HD,  $0 \leq \text{pH} \leq 13$ ) or from the pH 12.81 measured with a glass electrode designed for high pHs (Sentek P11,  $0 \leq \text{pH} \leq 14$ ), both calibrated with pH 7 and pH 10 buffers before use, but is in perfect agreement with the results of the PHREEQC calculation (pH 12.45; Table 1). At point C (ca. 50 min),  $\text{CO}_2$  was added to the Ar stream so that the partial pressure of  $\text{CO}_2$  in the cell atmosphere was 0.167 atm. A few seconds later, the potential began to rise steeply until it reached a second plateau. Since the electrode was well within its lifetime (the plateau for the  $\beta \rightarrow \alpha$  transition typically lasted 2 h for a 25  $\mu\text{m}$  diameter tip, the smallest electrode used in this study), this potential shift reflects a change in the local pH. The potential rise therefore corresponds to the acidification of the solution resulting from the neutralization of the  $\text{OH}^-$  ions from the lime, and the new plateau reflects the stabilization of the solution composition when all the  $\text{Ca}^{2+}$  ions have been consumed by the carbonation process, as described by equilibria 1–5 below:



Once all  $\text{Ca}^{2+}$  ions are consumed by reaction 5, the concentrations of all species from the carbonic acid system reach an equilibrium that depends on the partial pressure of  $\text{CO}_2$  in the atmosphere outside the porous mesh and on the solid phases produced by the carbonation (e.g., calcite and vaterite). In accordance with the calibration curve, the pH of the new plateau in Figure 3 is 6.34 (Table 2). The theoretical pH of a similar system as calculated by PHREEQC assuming formation of calcite is 6.50 (Table 1). Repetitions of the same test (Table 2) lead to a mean experimental value of  $6.46 \pm 0.06$ . The difference between this mean and the theoretical value,  $-0.04$ , therefore suggests that calcite is the most likely phase

**Table 2. Experimental pH Values Recorded at the End of the Carbonation of Saturated  $\text{Ca}(\text{OH})_2$  Solutions Confined in the Cellulose Mesh for Different  $p_{\text{CO}_2}$  and 23°C**

$p_{\text{CO}_2}$ (atm)	final pH at 23 °C (initial pH = 12.45)				
	1st test	2nd test	3rd test	average	standard error
0.750	6.13	6.06	6.17	6.12	0.03
0.167	6.34	6.56	6.47	6.46	0.06
0.039	6.95	6.78	6.85	6.86	0.05

formed. To ascertain which phase had precipitated, the mesh was observed using a SEM (to avoid further exposure to  $\text{CO}_2$ , the samples were initially dried in an Ar stream then in a drying oven under an Ar atmosphere and subsequently kept immersed in acetone). Figure 4 shows a zoom on a region illustrating the

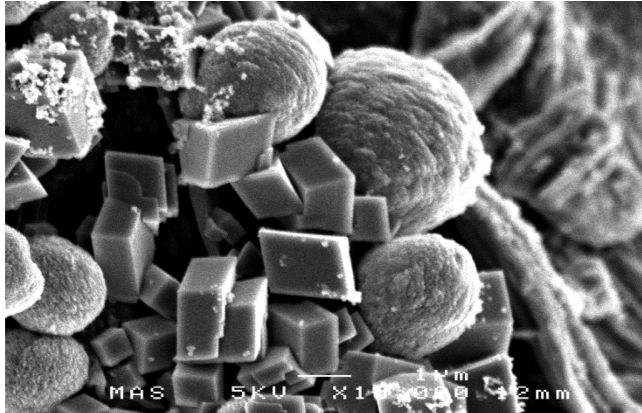


**Figure 4.** FE-SEM images of the cellulose mesh with calcite (rhombohedral) and vaterite (spherulites) crystals. The sample was previously coated with chromium to avoid charging in the SEM chamber.

morphologies of the two solid phases found on the cellulose fibers. The cubic crystals are characteristic of calcite formations, while the spherical crystals are characteristic of vaterite formations. This assignment was confirmed by X-ray diffraction as shown by the diffractograms in Figure SI-2 of the Supporting Information. The results of similar tests carried out with two other  $\text{CO}_2$  partial pressures, 0.039 and 0.750 atm, are reported in Table 2. All tests were repeated three times and in almost all cases, SEM analysis indicated that calcite was the main solid phase produced by the carbonation (Figure 5a); however, in one case the main solid phase formed was vaterite (Figure 5b). We surmise the crystallization of almost pure vaterite was related to the reaction kinetic because it was obtained in an experiment where the pH variation after the introduction of  $\text{CO}_2$  was unexpectedly fast compared with the other measurements (the second plateau was reached within a few min compared to over 30 min for experiments leading to calcite) and because vaterite is known to be an unstable phase evolving into calcite.<sup>48</sup> In Figure 6, we compare the experimental (filled symbols) and theoretical (empty symbols) dependence of the solution pH on the partial pressure of  $\text{CO}_2$  in the cell atmosphere. PHREEQC calculations were performed assuming the solution was in equilibrium with calcite (square symbols) and with vaterite (round symbols). In both cases, the pH decreases linearly with the logarithm of  $p_{\text{CO}_2}$ . All pH values determined from the microelectrode potentials are in very good agreement with the theoretical values calculated with

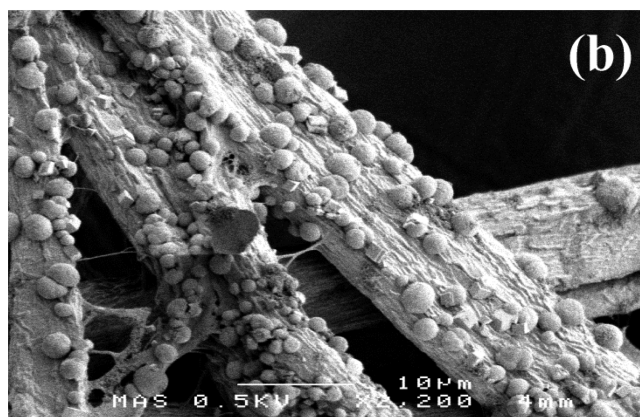
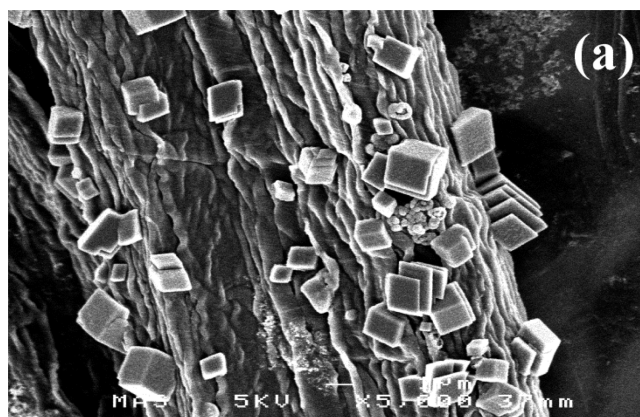


**Figure 5.** FE-SEM images of the sample fibers with (a) prevalent calcite crystals and (b) vaterite formations.

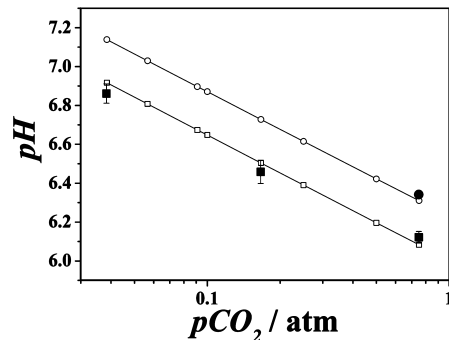


**Figure 6.** Dependence of the solution pH on the partial pressure of  $\text{CO}_2$  in the cell atmosphere. Theoretical (□) and experimental (■) results for calcite and theoretical (○) and experimental (●) results for vaterite.

PHREEQC. When calcite was found crystallized on the mesh fibers, the experimental pH values agree with the theoretical pH values obtained when the solution is in equilibrium with calcite. When vaterite was found crystallized on the fibers, the experimental pH is again in very good agreement with the theoretical pH for that phase. Remarkably, the experimental pH errors ( $\leq 0.06$  based on the three replicates shown in Table 2) are smaller than the difference between the theoretical pHs obtained when the solution is in equilibrium with vaterite and with calcite ( $\Delta\text{pH} = 0.22$ ), and it is thus possible to unequivocally assign the phase produced during carbonation from the microelectrode potential. From the slope of the E-pH relationship, the resolution is estimated to be better than a pH

of 0.02, while the comparison between experimental and theoretical results and the results shown in Table 2 suggest that the accuracy of the electrodes is better than a pH of 0.06.

To check the stability of the potentiometric response, we monitored the  $OCP_{\beta \rightarrow \alpha}$  potential of a 250  $\mu\text{m}$  diameter electrode continuously over 24 h in an Ar-purged saturated  $\text{Ca}(\text{OH})_2$  solution. Every 4 h, the Pd nanostructure was galvanostatically reloaded with hydrogen ( $-60 \mu\text{A}$  for 80 s) until a H/Pd ratio ca. 0.6 corresponding to the beginning of the  $\beta$  PdH phase. A new chronopotentiogram was recorded after each reloading sequence. In all cases, the plateau potential was found to be reproducible throughout the 24 h test.

## CONCLUSION

This study has demonstrated that pH microsensors made with nanostructured palladium hydride microelectrodes can operate reliably in very alkaline environments. Their potentiometric response was found to be Nernstian up to pH 14. To our knowledge, this is the first report of a pH microelectrode operating reliably at such high pH. We successfully employed the electrodes to monitor the change of pH during the carbonation of a saturated lime solution confined in a porous substrate exposed to a partial pressure of  $\text{CO}_2$ . The pH detected in situ was found to be in perfect agreement with theoretical calculations. The electrode response proved to be sufficiently sensitive and reproducible to differentiate, on the basis of pH, between the formation of calcite and vaterite, both polymorphs of calcium carbonate, inside the substrate. In this study, we focused on the potential plateaus and made no attempt to derive kinetic information from the shape and timescale of the potential transients. Preliminary observations indicate this is possible, and we are now planning to redesign the gas line to control more accurately the time when  $\text{CO}_2$  is introduced in the cell atmosphere. We believe these nanostructured pH microelectrodes are currently the only analytical tools capable of monitoring high pH in confined places and we expect they will be highly valuable to study geochemical processes involving very alkaline waters. It is worth stressing that as their response is clearly Nernstian from pH 1 to pH 14, these electrodes are not restricted to very high alkaline conditions and can also be applied to a multitude of processes. They are therefore highly suited as pH tips for scanning electrochemical microscopy and the monitoring of interfacial pH near solid and porous surfaces.

## ASSOCIATED CONTENT

### Supporting Information

Additional information as described in text. This material is available free of charge via the Internet at <http://pubs.acs.org>.

## AUTHOR INFORMATION

### Corresponding Author

\*E-mail: gd@soton.ac.uk.

### Notes

The authors declare no competing financial interest.

## ACKNOWLEDGMENTS

This work was funded by EPSRC Grants EP/I001204 and EP/I001956. G.D. also thanks the HanseWissenschaftskolleg, Institute for Advanced Study, Delmenhorst, Germany, for the fellowship.

## REFERENCES

- (1) Dole, M.; Wiener, B. *Z. J. Electrochem. Soc.* **1937**, *72*, 107.
- (2) Ives, D. J. G.; Janz, G. *Reference Electrodes*; Academic Press: New York, 1961.
- (3) Olson, R. A.; Tennis, P. D.; Bonen, D.; Jennings, H. M.; Mason, T. O.; Christensen, B. J.; Brough, A. R.; Sun, G. K.; Young, J. F. *J. Hazard Mater.* **1997**, *52*, 223.
- (4) Deslouis, C.; Frateur, I.; Maurin, G.; Tribollet, B. *J. Appl. Electrochem.* **1997**, *27*, 482.
- (5) Thili, M. M.; Benamor, M.; Gabrielli, C.; Perrot, H.; Tribollet, B. *J. Electrochem. Soc.* **2003**, *150*, C765.
- (6) Katsounaros, I.; Meier, J. C.; Klemm, S. O.; Topalov, A. A.; Biedermann, P. U.; Auinger, M.; Mayrhofer, K. J. *J. Electrochem. Commun.* **2011**, *13*, 634.
- (7) Davidovits, J. *Geopolymer Chemistry and Applications*, 3rd ed.; Geopolymer Institute: Saint-Quentin, France, 2011.
- (8) Glaus, M. A.; van Loon, L. R.; Achatz, S.; Chodura, A.; Fischer, K. *Anal. Chim. Acta* **1999**, *398*, 111.
- (9) VanLoon, L. R.; Glaus, M. A. *J. Environ. Polym. Degr.* **1997**, *5*, 97.
- (10) Caflisch, C. R.; Puccacco, L. R.; Carter, N. W. *Kidney Int.* **1978**, *14*, 126.
- (11) Caldwell, P. C. *Journal of Physiology* **1954**, *126*, 169.
- (12) Ha, Y.; Wang, M. *Electroanalysis* **2006**, *18*, 1121.
- (13) Izquierdo, J.; Nagy, L.; Varga, A.; Santana, J. J.; Nagy, G.; Souto, R. M. *Electrochim. Acta* **2011**, *56*, 8846.
- (14) Ha, Y.; Wang, M. *Rare Metal Materials and Engineering* **2006**, *35*, 261.
- (15) Avdic, A.; Lugstein, A.; Schondorfer, C.; Bertagnolli, E. *Appl. Phys. Lett.* **2009**, *95*, 223106.
- (16) Yamamoto, K.; Shi, G.; Zhou, T.; Xu, F.; Zhu, M.; Liu, M.; Kato, T.; Jin, J.-Y.; Jin, L. *Anal. Chim. Acta* **2003**, *480*, 109.
- (17) Kinoshita, E.; Ingman, F.; Edwall, G.; Thulin, S.; Glab, S. *Talanta* **1986**, *33*, 125.
- (18) Marzouk, S. A. M.; Ufer, S.; Buck, R. P.; Johnson, T. A.; Dunlap, L. A.; Cascio, W. E. *Anal. Chem.* **1998**, *70*, 5054.
- (19) Prats-Alfonso, E.; Abad, L.; Casan-Pastor, N.; Gonzalo-Ruiz, J.; Baldrich, E. *Biosens. Bioelectron.* **2013**, *39*, 163.
- (20) Nadappuram, B. P.; McKelvey, K.; Al Botros, R.; Colburn, A. W.; Unwin, P. R. *Anal. Chem.* **2013**, *85*, 8070.
- (21) Wang, Y.; Yuan, H. Y.; Lu, X. L.; Zhou, Z. D.; Xiao, D. *Electroanal.* **2006**, *18*, 1493.
- (22) da Silva, G. M.; Lemos, S. G.; Pocrifka, L. A.; Marreto, P. D.; Rosario, A. V.; Pereira, E. C. *Anal. Chim. Acta* **2008**, *616*, 36.
- (23) Colombo, C.; Kappes, T.; Hauser, P. C. *Anal. Chim. Acta* **2000**, *412*, 69.
- (24) Lima, A. C.; Jesus, A. A.; Tenan, M. A.; Silva, A.; Oliveira, A. F. *Talanta* **2005**, *66*, 225.
- (25) Razmi, H.; Heidari, H.; Habibi, E. *J. Solid State Electrochem.* **2008**, *12*, 1579.
- (26) Li, J. P.; Peng, T. Z.; Fang, C. *Anal. Chim. Acta* **2002**, *455*, 53.
- (27) Ekmekci, G.; Kalayci, S.; Somer, G. *Sens. Actuators, B* **2004**, *101*, 260.
- (28) Bakker, E.; Buhlmann, P.; Pretsch, E. *Chem. Rev.* **1997**, *97*, 3083.
- (29) Buhlmann, P.; Pretsch, E.; Bakker, E. *Chem. Rev.* **1998**, *98*, 1593.
- (30) Oesch, U.; Brzozka, Z.; Xu, A.; Rusterholz, B.; Suter, G.; Pham Hung, V.; Welti, D.; Ammann, D.; Pretsch, E.; Simon, W. *Anal. Chem.* **1986**, *58*, 2285.
- (31) Wencel, D.; Abel, T.; McDonagh, C. *Anal. Chem.* **2013**, *86*, 15.
- (32) Lukaszewski, M.; Czerwinski, A. *J. Solid State Electrochem.* **2011**, *15*, 2489.
- (33) Jasinski, R. *J. Electrochem. Soc.* **1975**, *122*, 1635.
- (34) Dobson, J. V.; Chapman, B. R.; Start, D. *J. Electrochem. Soc.* **1975**, *122*, 1634.
- (35) Jasinski, R. *J. Electrochem. Soc.* **1974**, *121*, 1579.
- (36) Dobson, J. V.; Brims, G. *Electrochim. Acta* **1987**, *32*, 149.
- (37) Dobson, J. V. *Platinum Metals Review* **1981**, *25*, 72.
- (38) Imokawa, T.; Williams, K. J.; Denuault, G. *Anal. Chem.* **2006**, *78*, 265.

- (39) Serrapede, M.; Denuault, G.; Sosna, M.; Pesce, G. L.; Ball, R. J. *Anal. Chem.* **2013**, *85*, 8341.
- (40) Parkhurst, D. L.; Appelo, C. A. J. *Description of Input and Examples for PHREEQC version 3: A Computer Program for Speciation, Batch-Reaction, One-Dimensional Transport, And Inverse Geochemical Calculations*; U.S. Geological Survey: Reston, VA, 2013.
- (41) Bartlett, P. N.; Gollas, B.; Guerin, S.; Marwan, J. *Phys. Chem. Chem. Phys.* **2002**, *4*, 3835.
- (42) Attard, G. S.; Bartlett, P. N.; Coleman, N. R. B.; Elliott, J. M.; Owen, J. R.; Wang, J. H. *Science* **1997**, *278*, 838.
- (43) Beynon, R. J.; Easterby, J. S. *Buffer Solutions: The Basics*; Taylor & Francis: Boca Raton, FL, 2003.
- (44) Cizer, O.; Rodriguez-Navarro, C.; Ruiz-Agudo, E.; Elsen, J.; Van Gemert, D.; Van Balen, K. *J. Mater. Sci.* **2012**, *47*, 6151.
- (45) Appelo, C. A. J.; Postma, D. *Geochemistry, Groundwater and Pollution*, 2nd ed.; Taylor & Francis: Boca Raton, FL, 2005.
- (46) Flanagan, T. B.; Oates, W. A. *Annu. Rev. Mater. Sci.* **1991**, *21*, 269.
- (47) Williams, K.-J. Development of a nanostructured palladium microelectrode for pH monitoring in scanning electrochemical microscopy. Ph.D. Thesis, University of Southampton, 2008.
- (48) Rodriguez-Blanco, J. D.; Shaw, S.; Benning, L. G. *Nanoscale* **2011**, *3*, 265.